All-Mode Quantum-Classical Path Integral Simulation of Bacteriochlorophyll Dimer Exciton-Vibration Dynamics

Amartya Bose[1,*] and Nancy Makri[1,2]

[1]*Department of Chemistry, University of Illinois, Urbana, Illinois 61801*
[2]*Department of Physics, University of Illinois, Urbana, Illinois 61801*

[*]*Present address: Department of Chemistry, Princeton University, Princeton, New Jersey 08540*

Abstract

We use the quantum-classical path integral (QCPI) methodology to report numerically exact, fully quantum mechanical results for the exciton-vibration dynamics in the bacteriochlorophyll dimer, including all 50 coupled vibrational normal modes of each bacteriochlorophyll explicitly with parameters obtained from spectroscopic Huang-Rhys factors. We present a coordinate transformation that maps the dimer on a spin-boson Hamiltonian with a single collective bath. We consider two vibrational initial conditions which correspond to a Franck-Condon excitation or to modes initially equilibrated with the excited monomer. Our calculations reveal persistent, underdamped oscillations of the electronic energy between the two pigments at room temperature. Static disorder leads to additional damping, but the population dynamics remains oscillatory. The population curves exhibit atypical, nonsmooth features that arise from the complexity of the bacteriochlorophyll vibrational spectrum and which cannot be captured by simple analytical spectral density functions.

I. Introduction

The fascinating details of photosynthesis[1,2] continue to attract intense theoretical and experimental efforts. Besides the desire to fully understand the mechanistic pathways of this intriguing process, much of this work is driven by technological interest, namely the prospect of mimicking nature to design highly efficient energy harvest and storage devices.

In particular, the specifics of excitation energy transfer (EET) following the absorption of a photon by the light harvesting pigment-protein complexes of plants and photosynthetic bacteria continues to pose a number of questions. At the central focus of current investigations is the inter-pigment energy transfer dynamics in the B850 ring of the light harvesting complex II, and also in the Fenna–Matthews–Olson (FMO) complex.[3,4] In purple bacteria, the former (LH2 complex) consists of 16 or 18 dimerized bacteriochlorophyll (BChl) *a* units, which are strongly coupled to their nearest neighbors. In the perfectly symmetric ring, the electronic eigenstates are coherently delocalized among all dimers. Static disorder from the ring's environment introduces a variation of the site energies. If strong, this asymmetry can lead to partially or fully localized eigenstates. The FMO complex is a trimer composed of seven BChl molecules. The near-unity quantum yield of the energy transfer process has prompted much discussion regarding the nature of EET in these systems.

The optical and vibronic properties of individual BChl molecules and of light harvesting complexes have been studied extensively using absorption/emission, spectral hole burning, fluorescence line narrowing, resonant Raman and time-resolved techniques.[5-13] Experimental studies of the light harvesting BChl aggregates have reported intriguing patterns. In the late 1990s, fluerescence anisotropy experiments reported quantum beating in FMO.[14] In recent years, time-resolved two-dimensional spectroscopic techniques[15,16] have revealed long-lived oscillatory patterns in FMO and LH2 complexes.[17,18] The origin of these oscillations continues to be hotly debated.[19-27]

Theoretical studies of EET in light harvesting complexes[13,19-22,26,28-41] have focused on obtaining electroning coupling parameters and calculating population evolution or nonlinear spectra through third-order response functions[42] in model Hamiltonians. The majority of the time-dependent calculations employ a tight-binding Hamiltonian describing the singly excited BChl electronic states that participate in the energy transfer process, while the vibrational modes of the chromophores and surrounding medium are typically included as a harmonic bath characterized by a model spectral density. In the past, the majority of simulations on FMO or LH2 aggregates have focused on investigating the behaviors resulting from various parameter choices.

However, even with the harmonic bath simplification, accurate treatment of quantum dynamical evolution of is all but straightforward. Beyond perturbative and Markovian master equation treatments,[43,44] simulations of system-bath dynamics typically follow one of two avenues. The first is based on the Meyer-Miller mapping Hamiltonian approach,[45,46] which replaces the discrete electronic states by continuous degrees of freedom. This approach allows a unified treatment of the electronic and nuclear coordinates via classical trajectories within linearized semiclassical initial value methods.[47] The second avenue retains the discrete nature of the electronic states and treats the harmonic bath degrees of freedom via real-time path integral methods or hierarchical equations of motion. The latter approach[48] is restricted to a model spectral density of the Drude form, which represents a Brownian oscillator and thus is unable to treat the complex spectral characteristics of the chlorophyll vibrations.

The path integral formulation of time-dependent quantum mechanics[49,50] offers an elegant and intuitive approach, which is ideally suited to system-bath Hamiltonians.[51] This is so because the contributions from a harmonic bath to the reduced density matrix of the system can be integrated out exactly within the path itnegral framework, giving rise to the Feynman-Vernon influence functional.[52] The quasiadiabatic propagator path integral (QuAPI) methodology[53-55] is a numerically exact algorithm that can treat baths of arbitrary spectral densities. It involves an iterative algorithm which treats explicitly only the system path segments within the bath-induced memory length, leading to linear scaling with the number of time steps. However, the path array that spans the memory length can become very large when multistate systems are involved or if the memory is very long. A number of techniques have been developed[56-61] for reducing the size of this array, and the resulting size reduction can be dramatic in some regimes. In the incoherent regime (i.e. at high temperature and with strong system-bath coupling), the blip decomposition[62,63] offers exponential acceleration of the path sum, offering an efficient approach in situations of very long memory. Most recently, it was shown that the path integral variables can be disentangled even within the memory length, leading to a small matrix path integral[64] (SMatPI) algorithm which requires storage of matrices whose size is that of the bare system. As a result, the SMatPI decomposition allows fully quantum mechanical calculations in systems with multiple states.

Recent efforts have led to the development of algorithms suitable for simulating processes in anharmonic media. The mixed quantum-classical Liouville equation,[65,66] in particular its momentum-jump formulation,[67,68] is a rigorous approach, but the computational demands of the method increase exponentially with propagation time. Unlike quantum-classical methods based on wavefunctions, which involve *ad hoc* assumptions dictated by the need to correct the shortcomings of the Ehrenfest mean field model,[69] the path integral representation allows a consistent treatment of a discrete quantum system and the classical degrees of freedom that constitute its environment. This is a consequence of the local, trajectory-like nature of quantum paths, which allows the treatment of the interaction between quantum and classical degrees of freedom without approximation and in full atomistic detail. The quantum-classical path integral[70-72] (QCPI) methodology offers a rigorous formulation that correctly captures the decoherence induced by the classical degrees of freedom through destructive interference of quantum-semiclassical phase factors. The algorithm scales linearly with propagation length and has been shown to be practical for simulating nonadiabatic processes in solution[73] without *ad hoc* assumptions or adjustable parameters. Last, the modular decomposition of the path integral[74,75] offers linear scaling with system size in extended systems characterized by a one-dimensional topology.

The QCPI expression becomes exact in the case of a harmonic bath, and thus offers yet another alternative to influence functional-based methods. Because the classical component of the bath-induced memory is captured automatically in the QCPI propagator,[76] the algorithm needs to account only for the residual quantum memory effects, which are much weaker. For this reason, the QCPI methodology converges faster, thus allowing simulations in more challenging regimes.

The EET dynamics of biological antenna complexes involves electronic and vibrational motions of comparable timescales, couplings of intermediate strength, and vibrational modes that induce long memory. As a result, simulation of the time evolution with the true molecular parameters that characterize these systems face serious challenges. In this work we report QCPI simulations of the energy transfer dynamics in BChl dimers, including the normal mode vibrations of each unit with highly accurate parameters obtained from spectroscopic Huang-Rhys factors that have been obtained from Q_y fluorescence emission spectra of *Rhodobacter sphaeroides* using difference fluorescence line narrowing.[13]

In section II we describe the BChl dimer Hamiltonian. Starting from the ground and excited states of a single BChl, which are expressed in terms of the normal mode coordinates with parameters given in terms of Huang-Rhys factors, we perform a transformation that brings the dimer to the conventional spin-boson form. In section III we discuss two possible initial conditions for the vibrational modes, and describe its transformation to the new coordinates. In section IV we extend the description to include the effects of static disorder mimicking a sluggish protein environment. An overview of the QCPI algorithm, along with the various parameters we consider, are given in section V. The results of our simulations are presented and discussed in section VI. Section VII concludes with a disucssion and additional remarks.

II. The chlorophyll dimer Hamiltonian

Each BChl pigment is modeled in terms of two electronic states $|0\rangle$ and $|1\rangle$ describing the $S_0 \to S_1$ transition that corresponds to the Q_y band. Thus the electronic Hamiltonian for a single BChl molecule is $E_0 |0\rangle\langle 0| + E_1 |1\rangle\langle 1|$, where E_0, E_1 are the electronic eigenvalues. When vibrational degrees of freedom are considered, the Hamiltonian for BChl α becomes

$$\hat{H}^{\alpha} = \left(E_0^{\alpha} + \hat{h}_{0,\mathrm{vib}}^{\alpha}\right)\left|0^{\alpha}\right\rangle\left\langle 0^{\alpha}\right| + \left(E_1^{\alpha} + \hat{h}_{1,\mathrm{vib}}^{\alpha}\right)\left|1^{\alpha}\right\rangle\left\langle 1^{\alpha}\right|, \tag{2.1}$$

where identity operators in the electronic and vibrational subspaces have been omitted for notational simplicity. Within the normal mode approximation, the vibrational Hamiltonians $h_{0,\mathrm{vib}}^{\alpha}$ and $h_{1,\mathrm{vib}}^{\alpha}$ are given by quadratic forms. If the minimum energy geometry of the ground state is set to zero, the vibrational Hamiltonian has the usual quadratic form

$$\hat{h}_{0,\mathrm{vib}}^{\alpha} = \sum_{j=1}^{n} \frac{\left(\hat{p}_j^{\alpha}\right)^2}{2m} + \frac{1}{2} m\omega_j^2 \left(\hat{q}_j^{\alpha}\right)^2 \tag{2.2}$$

where $m = 1$ and $q_j^{\alpha}, p_j^{\alpha}$ denote the normal mode coordinates and momenta of monomer α. The ground and excited state geometries are very similar, leading to very similar normal mode frequencies on the two electronic states and a very small Duschinskin rotation,[13] which typically is neglected. Thus the excited state Hamiltonian has the form

$$\hat{h}_{1,\mathrm{vib}}^{\alpha} = \sum_{j=1}^{n} \frac{\left(\hat{p}_j^{\alpha}\right)^2}{2m} + \frac{1}{2} m\omega_j^2 \left(\hat{q}_j^{\alpha} - d_j\right)^2 = \hat{h}_{0,\mathrm{vib}}^{\alpha} - m\omega_j^2 d_j \hat{q}_j^{\alpha} + \frac{1}{2} m\omega_j^2 d_j^2 . \tag{2.3}$$

While each BChl pigment has it own vibrational coordinates, the normal mode frequencies ω_j and displacements d_j are the same for both BChl molecules. Accurate parameters for the BChl vibrational modes of *Rhodobacter sphaeroides* have been determined from Q_y fluorescence emission spectra.[13] The displacement distances d_j of the $n = 50$ normal modes that have non-negligible couplings[13] are related to the Huang-Rhys factors,

$$D_j = \frac{m\omega_j}{2\hbar} d_j^2 . \tag{2.4}$$

Consider a BChl dimer consisting of two monomers, labeled A and B. Energy transfer in molecular aggregates[77] is often conveniently described by the well-known Frenkel exciton Hamiltonian,[78]

$$\hat{H}^{\mathrm{AB}} = \hat{H}^{\mathrm{A}} + \hat{H}^{\mathrm{B}} + \hat{V}^{\mathrm{AB}} . \tag{2.5}$$

Here the two monomers are coupled via the term

$$\hat{V}^{\mathrm{AB}} = -J\left(\left|0^{\mathrm{A}}1^{\mathrm{B}}\right\rangle\left\langle 1^{\mathrm{A}}0^{\mathrm{B}}\right| + \left|1^{\mathrm{A}}0^{\mathrm{B}}\right\rangle\left\langle 0^{\mathrm{A}}1^{\mathrm{B}}\right|\right), \tag{2.6}$$

where $J > 0$ is the exciton coupling parameter.

Upon simplifying, the Hamiltonian can be written as a sum of zero-excitation, single excitation and double excitation terms. In fact, these subspaces are completely uncoupled from each other. At ordinary light intensities, it is sufficient to restrict attention to the single excitation Frenkel subspace, whose Hamiltonian is

$$\begin{aligned}\hat{H}_{\mathrm{single}} = &\left(E_1^{\mathrm{A}} + \hat{h}_{1,\mathrm{vib}}^{\mathrm{A}} + E_0^{\mathrm{B}} + \hat{h}_{0,\mathrm{vib}}^{\mathrm{B}}\right)\left|1^{\mathrm{A}}0^{\mathrm{B}}\right\rangle\left\langle 1^{\mathrm{A}}0^{\mathrm{B}}\right| + \left(E_0^{\mathrm{A}} + \hat{h}_{0,\mathrm{vib}}^{\mathrm{A}} + E_1^{\mathrm{B}} + \hat{h}_{1,\mathrm{vib}}^{\mathrm{B}}\right)\left|0^{\mathrm{A}}1^{\mathrm{B}}\right\rangle\left\langle 0^{\mathrm{A}}1^{\mathrm{B}}\right| \\ &-J\left(\left|0^{\mathrm{A}}1^{\mathrm{B}}\right\rangle\left\langle 1^{\mathrm{A}}0^{\mathrm{B}}\right| + \left|1^{\mathrm{A}}0^{\mathrm{B}}\right\rangle\left\langle 0^{\mathrm{A}}1^{\mathrm{B}}\right|\right)\end{aligned} \tag{2.7}$$

Defining the state with chlorophyll A excited as 'right', and that with chlorophyll B excited as 'left', i.e.,

$$\left|R\right\rangle \equiv \left|1^{\mathrm{A}}0^{\mathrm{B}}\right\rangle,\ \left|L\right\rangle \equiv \left|0^{\mathrm{A}}1^{\mathrm{B}}\right\rangle, \tag{2.8}$$

dropping additive constants and simplifying the expression, the single excitation Hamiltonian becomes

$$\hat{H}_{\mathrm{single}} = \hat{H}_0 + \hat{h}_{0,\mathrm{vib}}^{\mathrm{A}} + \hat{h}_{0,\mathrm{vib}}^{\mathrm{B}} - \sum_{j=1}^{n} m\omega_j^2 d_j \left(\hat{q}_j^{\mathrm{A}}\left|R\right\rangle\left\langle R\right| + \hat{q}_j^{\mathrm{B}}\left|L\right\rangle\left\langle L\right|\right) \tag{2.9}$$

with

$$\hat{H}_0 = \left(E_1^{\mathrm{A}} + E_0^{\mathrm{B}}\right)\left|R\right\rangle\left\langle R\right| + \left(E_0^{\mathrm{A}} + E_1^{\mathrm{B}}\right)\left|L\right\rangle\left\langle L\right| - J\left(\left|R\right\rangle\left\langle L\right| + \left|L\right\rangle\left\langle R\right|\right) = -J\left(\left|R\right\rangle\left\langle L\right| + \left|L\right\rangle\left\langle R\right|\right), \tag{2.10}$$

where the second equality follows by noting that for the isolated dimer $E_0^{\mathrm{A}} + E_1^{\mathrm{B}} = E_1^{\mathrm{A}} + E_0^{\mathrm{B}}$, and readjusting the zero of energy.

Eq. (2.9) is a Hamiltonian for two states coupled to a doubly degenerate harmonic bath, but it is not in the usual spin-boson form. Instead, the R state corresponds to a surface centered about $q_j^{\mathrm{A}} = d_j,\ q_j^{\mathrm{B}} = 0$, while the L state corresponds to a parabolic potential surface centered about $q_j^{\mathrm{A}} = 0,\ q_j^{\mathrm{B}} = d_j$. These surfaces are illustrated in Figure 1 for same-frequency normal modes of the two monomers. This arrangement of the vibrational potential surfaces suggests the transformation

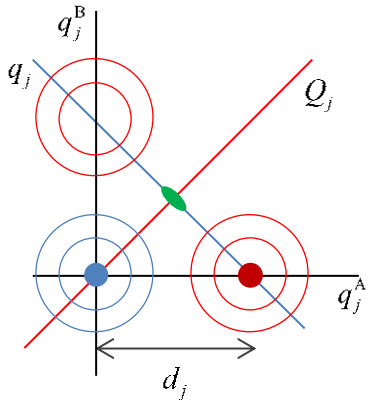

Fig. 1. Schematic illustration of normal mode potential surfaces and coordinate transformation for a single vibrational mode of the ground (blue) and the two singly excited (red) monomers in the chlorophyll dimer. The shaded blue and red circles illustrate the vibrational density for initial conditions (i) and (ii). The shaded green ellipse (the projection of the blue circle) indicates the vibrational density in the space of the coupled difference normal mode coordinate for initial condition (i).

$$Q_j = \frac{1}{\sqrt{2}}\left(q_j^{\mathrm{A}} + q_j^{\mathrm{B}}\right), \quad q_j = \frac{1}{\sqrt{2}}\left(q_j^{\mathrm{A}} - q_j^{\mathrm{B}}\right). \tag{2.11}$$

In these new coordinates, the single excitation Hamiltonian becomes

$$\begin{aligned} \hat{H}_{\mathrm{single}} = \hat{H}_0 &+ \sum_{j=1}^{n}\left(\frac{\hat{P}_j^2}{2m} + \frac{1}{2}m\omega_j^2\hat{Q}_j^2 - \frac{d_j}{\sqrt{2}}m\omega_j^2\hat{Q}_j\right) \\ &+ \sum_{j=1}^{n}\left(\frac{\hat{p}_j^2}{2m} + \frac{1}{2}m\omega_j^2\hat{q}_j^2 - \frac{d_j}{\sqrt{2}}m\omega_j^2\hat{q}_j\left(|R\rangle\langle R| - |L\rangle\langle L|\right)\right) \end{aligned} \tag{2.12}$$

where P_j and p_j are the corresponding conjugate momenta.

As can be seen in Fig. 1, the sum coordinate Q_j is not coupled to the electronic states. Thus this coordinate does not play a role in the energy transfer and can be removed from the dimer Hamiltonian. The potential minima of the singly excited states lie along the q_j coordinate and are shifted by $d_j/\sqrt{2}$ when the dimer is in the *R* state, and by $-d_j/\sqrt{2}$ when the dimer is in the *L* state. After dropping the uncoupled Q_j terms, the chlorophyll dimer Hamiltonian takes the familiar spin-boson form

$$\hat{H} = -J\hat{\sigma}_x + \sum_{j=1}^{n}\left(\frac{1}{2}\hat{p}_j^2 + \frac{1}{2}m\omega_j^2\hat{q}_j^2 - c_j\hat{q}_j\hat{\sigma}_z\right) \equiv \hat{H}_0 + \hat{H}_{\mathrm{env}}\ , \tag{2.13}$$

where $\hat{H}_0 = -J\hat{\sigma}_x$ is the electronic part, $c_j = d_j m\omega_j^2/\sqrt{2}$, and σ_x, σ_z are the usual Pauli spin matrices. In this Hamiltonian, the couplings to the "bath" are reduced from those in a single chlorophyll by a factor of $\sqrt{2}$. The reason for this decrease is the increase in the actual distance between the vibrational

potential minima, which (as seen from Fig. 1) is given by the hypotenuse of the triangle, while the distance of the coordinates corresponding to left and right states in Eq. (2.13) remains equal to 2. The chlorophyll dimer Hamiltonian is similar to the form employed by Tiwari *et. al.*, [24] which was suggested based on physical arguments pertaining to symmetric and antisymmetric vibrations.

III. Initial conditions

We assume that at $t = 0$, BChl A is placed in the excited electronic state, i.e., the initial density matrix is given by

$$\hat{\rho}^{\mathrm{AB}}(0) = \left|1^{\mathrm{A}}0^{\mathrm{B}}\right\rangle\left\langle 1^{\mathrm{A}}0^{\mathrm{B}}\right| \hat{\rho}^{\mathrm{AB}}_{\mathrm{vib}}(0)\,, \tag{3.1}$$

and consider the following two possibilities for the vibrational degrees of freedom:

(i) Franck-Condon excitation. The vibrational modes of each BChl are initially in equilibrium with the ground electronic state of that monomer,

$$\hat{\rho}^{\mathrm{AB}}_{\mathrm{vib}}(0) = e^{-\beta \hat{h}^{\mathrm{A}}_{0,\mathrm{vib}}} e^{-\beta \hat{h}^{\mathrm{B}}_{0,\mathrm{vib}}}\,, \tag{3.2}$$

where $\beta = 1/k_{\mathrm{B}}T$ is the reciprocal temperature. This initial condition is consistent with a Franck-Condon transition. The matrix element of the Boltzmann operator for the quadratic vibrational modes of BChl α in its ground electronic state has the form[79]

$$\left\langle \mathbf{q}'^{\alpha}\left| e^{-\beta \hat{h}^{\alpha}_{0,\mathrm{vib}}}\right| \mathbf{q}^{\alpha}\right\rangle = \kappa \prod_{j=1}^{n} \exp\left[-\lambda_j \left(q'^{\alpha}_j\right)^2 - \lambda_j \left(q^{\alpha}_j\right)^2 - \mu_j q'^{\alpha}_j q^{\alpha}_j\right] \tag{3.3}$$

where κ, λ_j and μ_j are constants that depend on the mode frequencies and the temperature. Using the coordinate transformation relations of section II, we obtain

$$\left(q^{\mathrm{A}}_j\right)^2 + \left(q^{\mathrm{B}}_j\right)^2 = Q^2_j + q^2_j\,, \qquad q'^{\mathrm{A}}_j q^{\mathrm{A}}_j + q^{\mathrm{B}}_j q'^{\mathrm{B}}_j = Q'_j Q_j + q'_j q_j\,. \tag{3.4}$$

Multiplying the Boltzmann operator matrix elements for the two monomers and using Eq. (3.4), we arrive at the result

$$\left\langle \mathbf{q}'^{\mathrm{A}}\left| e^{-\beta \hat{h}^{\mathrm{A}}_{0,\mathrm{vib}}}\right| \mathbf{q}^{\mathrm{A}}\right\rangle \left\langle \mathbf{q}'^{\mathrm{B}}\left| e^{-\beta \hat{h}^{\mathrm{B}}_{0,\mathrm{vib}}}\right| \mathbf{q}^{\mathrm{B}}\right\rangle = \kappa^2 \exp\left[-\lambda_j\left(Q^2_j + q^2_j + Q'^2_j + q'^2_j\right) - \mu_j\left(Q'_j Q_j + q'_j q_j\right)\right]. \tag{3.5}$$

Since only the difference coordinates contribute to the dynamics, the vibrational component of the initial density is

$$\kappa \exp\left[-\lambda_j\left(q'^2_j + q^2_j\right) - \mu_j q'_j q_j\right] = \left\langle \mathbf{q}'\left| e^{-\beta \hat{h}^{\mathrm{unshifted}}_{\mathrm{bath}}}\right| \mathbf{q}\right\rangle, \tag{3.6}$$

i.e. the density operator for the bath is given by

$$\hat{\rho}_{\rm vib}^{\rm (i)}(0) = \frac{e^{-\beta \hat{h}_{\rm bath}^{\rm unshifted}}}{{\rm Tr}\, e^{-\beta \hat{h}_{\rm bath}^{\rm unshifted}}} \tag{3.7}$$

where

$$\hat{h}_{\rm bath}^{\rm unshifted} = \sum_{j=1}^{n} \left(\frac{\hat{p}_j^2}{2m} + \frac{1}{2} m\omega_j^2 \hat{q}_j^2 \right) \tag{3.8}$$

is the Hamiltonian for the bath degrees of freedom in Eq. (2.13). The density of Eq. (3.6) is shown schematically in Fig. 1.

(ii) Equilibrated excited state. As a second possibility, the vibrational modes of the initially excited BChl are assumed to have equilibrated with the excited electronic state of that pigment prior or the onset of dynamics on the singly excited Hamiltonian, i.e.,

$$\hat{\rho}_{\rm vib}^{\rm AB}(0) = e^{-\beta \hat{h}_{1,\rm vib}^{\rm A}} e^{-\beta \hat{h}_{0,\rm vib}^{\rm B}} \,. \tag{3.9}$$

In this case the Boltzmann matrix element for pigment A is given

$$\left\langle \mathbf{q}'^{\rm A} \left| e^{-\beta \hat{h}_{1,\rm vib}^{\rm A}} \right| \mathbf{q}^{\rm A} \right\rangle = \kappa \prod_{j=1}^{n} \exp\left[-\lambda_j \left(q_j'^{\alpha} - d_j \right)^2 - \lambda_j \left(q_j^{\alpha} - d_j \right)^2 - \mu_j \left(q_j'^{\alpha} - d_j \right)\left(q_j^{\alpha} - d_j \right) \right], \tag{3.10}$$

while for pigment B it still has the form of Eq. (3.3). Using again the coordinate transformations of the previous section and performing some straightforward algebra, we find

$$\begin{aligned} &\left\langle \mathbf{q}'^{\rm A} \left| e^{-\beta \hat{h}_{1,\rm vib}^{\rm A}} \right| \mathbf{q}^{\rm A} \right\rangle \left\langle \mathbf{q}'^{\rm B} \left| e^{-\beta \hat{h}_{0,\rm vib}^{\rm B}} \right| \mathbf{q}^{\rm B} \right\rangle \\ &= \kappa^2 \exp\left[-\lambda_j \left(Q_j' - \frac{d_j}{\sqrt{2}} \right)^2 - \lambda_j \left(Q_j - \frac{d_j}{\sqrt{2}} \right)^2 - \lambda_j \left(q_j' - \frac{d_j}{\sqrt{2}} \right)^2 - \lambda_j \left(q_j - \frac{d_j}{\sqrt{2}} \right)^2 \right] \\ &\times \exp\left[-\mu_j \left(Q_j - \frac{d_j}{\sqrt{2}} \right)\left(Q_j' - \frac{d_j}{\sqrt{2}} \right) - \mu_j \left(q_j' - \frac{d_j}{\sqrt{2}} \right)\left(q_j - \frac{d_j}{\sqrt{2}} \right) \right] \end{aligned} \tag{3.11}$$

One sees that the contribution of the coupled difference coordinate is

$$\kappa \exp\left[-\lambda_j \left(q_j' - \frac{d_j}{\sqrt{2}} \right)^2 - \lambda_j \left(q_j - \frac{d_j}{\sqrt{2}} \right)^2 - \mu_j \left(q_j' - \frac{d_j}{\sqrt{2}} \right)\left(q_j - \frac{d_j}{\sqrt{2}} \right) \right] = \left\langle \mathbf{q}' \left| e^{-\beta \hat{h}_{\rm bath}^{\rm shifted}} \right| \mathbf{q} \right\rangle, \tag{3.12}$$

i.e. the density operator for the bath is given by

$$\hat{\rho}_{\text{vib}}^{(\text{ii})}(0) = \frac{e^{-\beta \hat{h}_{\text{bath}}^{\text{shifted}}}}{\text{Tr}\, e^{-\beta \hat{h}_{\text{bath}}^{\text{shifted}}}} \tag{3.13}$$

where

$$\hat{h}_{\text{bath}}^{\text{shifted}} = \sum_{j=1}^{n} \left[\frac{\hat{p}_j^2}{2m} + \frac{1}{2} m\omega_j^2 \left(\hat{q}_j - \frac{d_j}{\sqrt{2}} \right)^2 \right], \tag{3.14}$$

i.e. the initial state is in this case the Boltzmann distribution for the effective bath modes in equilibrium with the initially excited *R*-localized electronic state.

IV. Static disorder

Chlorophyll molecules are integral components of the photosynthesic apparatus of plants and bacteria, where they are embedded in light harvesting chrlorophyll-protein complexes. The present treatment of the BChl vibrations in terms of normal modes, with parameters obtained from experimental Huang-Rhys factors, does not allow embedding the BChl dimer in its protein scaffold. The slow motions of the protein (those which occur on time scales much longer than those of EET dynamics) are commonly modeled as a static disorder, which affects the energies of the two exciton states by varying amounts. In addition to presenting accurate quantum mechanical results for the symmetric dimer, in the next section we report a qualititave picture of the effects of sluggish protein motion by accounting for static disorder in the exciton-vibration dynamics. We emphasize that the static treatment of disorder cannot account for the dissipative effects of phonon-like protein degrees of freedom on the population dynamics of the BChl dimer. If protein fluctuations were to be included, the dephasing effects from a large number of modes with characteristic times of the order of the EET would lead to additional quenching of the oscillatory patterns observed in our calculations.

To this end, we return to Eq. (2.10) and allow the ground and excited state energies of the two BChl monomers to differ. Defining the parameter $\varepsilon = \frac{1}{2}\left[\left(E_1^{\text{A}} - E_0^{\text{A}} \right) - \left(E_1^{\text{B}} - E_0^{\text{B}} \right) \right]$ (i.e. half the excitation energy of the two molecules) and adjusting the zero of energy, the singly excited electronic Hamiltonian becomes

$$\hat{H}_0 = \varepsilon \left(|R\rangle\langle R| - |L\rangle\langle L| \right) - J \left(|R\rangle\langle L| + |L\rangle\langle R| \right) = -J\sigma_x + \varepsilon\sigma_z \ . \tag{4.1}$$

In the calculations presented in the next two sections we assume that the excitation energy difference is normally distributed around its mean value $\bar{\varepsilon}$, with a standard deviation σ.

V. Parameters and methods

Rätsep *et. al.*[13] have reported Huang-Rhys factors for the electron-phonon couplings for the 50 most strongly coupled BChl vibrational modes. These parameters were used to determine the ground-

excited state mode displacements and thus the coupling coefficients in Eq. (2.13). The collective effects of the bath are captured in the spectral density function,

$$J(\omega)=\frac{\pi}{2}\sum_j \frac{c_j^2}{m_j\omega_j}\delta(\omega-\omega_j) \tag{5.1}$$

The spectral density of the bath corresponding to the transformed BChl dimer Hamiltonian of Eq. (2.13) is shown if Figure 2. It is clear that the intricate structure of the BChl spectral density cannot be accounted for by simple analytical models.

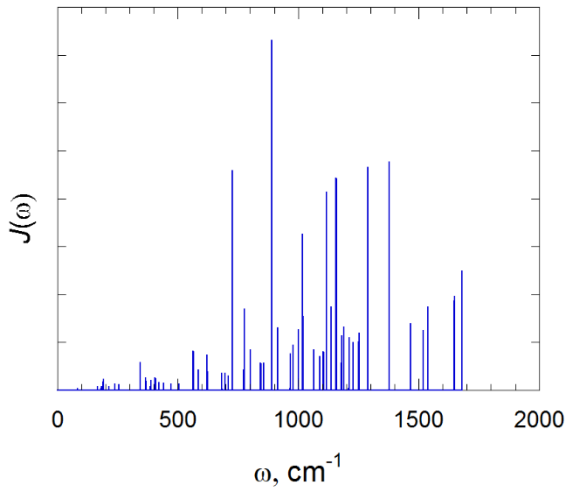

Fig. 2. Spectral density for the bacteriochlorophyll dimer (in arbitrary units).

For the isolated BChl dimer, the only other parameter needed is the electronic coupling J. A number of methods have been used to compute this parameter in the antenna complexes of photosynthetic bacteria. For LH2, most reported values are in the range 200-400 cm^{-1} range. In this work we present results with the intra-dimer coupling parameter $J=363\,\mathrm{cm}^{-1}$ obtained by Tretiak and Mukamel[29] and also for the intra- and inter-dimer coupling values 315 and 245 cm^{-1} reported by Freiberg *et al.* [80] We also present calculations for a smaller value of the electronic coupling, $J=181\,\mathrm{cm}^{-1}$. The standard deviation for the static disorder parameter is $\sigma=220\,\mathrm{cm}^{-1}$.[80]

The reduced density matrix that corresponds to Eq. (2.13) is given by

$$\tilde{\rho}_{ij}(t)=\mathrm{Tr}_{\mathrm{vib}}\langle i|e^{-i\hat{H}t/\hbar}\hat{\rho}(0)e^{i\hat{H}t/\hbar}|j\rangle,\quad i,j=R,L \tag{5.2}$$

The diagonal elements of Eq. (5.2) give the populations of the two BChl excited states, the population $P(t)$ of the excited state of BChl A is given by

$$P(t)=\tilde{\rho}_{RR}(t). \tag{5.3}$$

For an initial state corresponding to the excitation localized on monomer A, the initial density operator has the form

$$\hat{\rho}(0) = |R\rangle\langle R| \frac{e^{-\beta \hat{h}_{\text{bath}}}}{\text{Tr} e^{-\beta \hat{h}_{\text{bath}}}} \tag{5.4}$$

where, according to the results of section III, the bath Hamiltonian is either unshifted or shifted.

The populations of the two exciton states are obtained using the quantum-classical path integral methodology. The QCPI formulation[70-72] involves summing the amplitudes of the quantum paths of the two-state system, which are augmented by semiclassical phases obtained along classical trajectories. Each classical trajectory hops between the two electronic states as dictated by a particular quantum path, thus the number of trajectories from each phase space initial condition is equal to the number of paths of the electronic system. The memory quenching effects of the environment are exploited to prevent the exponential proliferation of trajectories.[76,81,82] Once converged with respect to the path integral time step and the memory time, the QCPI expression produces rigorous quantum-classical results, which are free of any assumptions or adjustable parameters. The integration with respect to trajectory initial conditions is performed using Metropolis sampling[83] with 35,000 initial conditions.

In the particular case of a harmonic bath, the QCPI formulation reverts to the full quantum mechanical expression.[70] Since the BChl vibrations are treated in terms of normal modes which involve a quadratic potential function, the QCPI calculations on the BChl dimer produce numerically exact results. Further acceleration of the calculation for this harmonic environment is possible by exploiting the cumulative treatment of the harmonic bath back-reaction.[84,85] The phase space average with respect to trajectory initial conditions is performed via Metropolis sampling.[83]

The QCPI results presented in the next section converged with a time step equal to 4.84 fs. The QCPI calculations were performed with a memory length equal to 48.38 fs in the case of initial condition (i), and 29.04 fs for initial condition (ii).

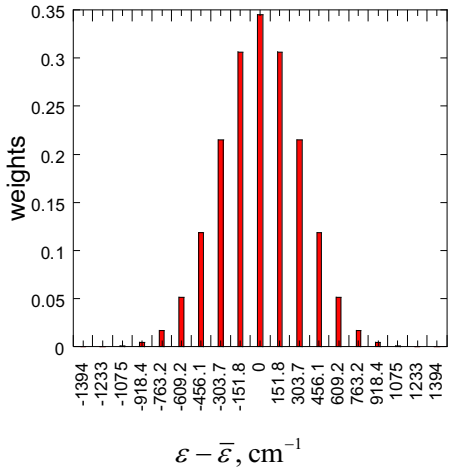

Fig. 3. Weights corresponding to various different asymmetries obtained using a Gauss-Hermite discretization.

The effects of static disorder are included by averaging the QCPI population results with respect to the excitation energy difference ε, assuming[36] that the energy of the excited state of each of the chlorophyll monomers follows a Gaussian distribution with mean equal to $\bar{\varepsilon}$ and standard deviation $\sigma = 220\,\mathrm{cm}^{-1}$.[80] Therefore the excitation energy difference 2ε is sampled from a Gaussian with standard deviation $\sqrt{2} \times 220\,\mathrm{cm}^{-1}$.

The average over the asymmetry parameter is performed using a Gauss-Hermite quadrature with 41 grid points. Figure 3 shows a histogram of the points, along with their weights. It is seen that only 13 grid points have a weight greater than 0.001. We have performed calculations for these points and averaged the obtained populations.

VI. Exciton population dynamics

In this section we present the results of our calculations. Figure 4 shows the population dynamics of the BChl A excited state for a symmetric dimer (i.e., $\varepsilon = 0$) at $T = 300\,\mathrm{K}$ for the electronic coupling values $J = 363, 315, 245, 181\,\mathrm{cm}^{-1}$.[30,80] The tunneling splitting of the electronic state doublet is equal to $2J$, which for $J = 363\,\mathrm{cm}^{-1}$ corresponds to an oscillation with period ~54 fs. The coupled vibrations introduce dissipative effects, and the electronic populations exhibit underdamped oscillations. Decreasing the value of J slows down the population oscillations and leads to faster damping, as the coupling to the decohering vibrations is effectively stronger for a smaller value of the electronic coupling.

The two initial conditions discussed in section III are seen to lead to small differences in the dynamics, which are more prominent at short times. With the Franck-Condon initial condition (i), the density of the vibrational modes is initially in between the potential minima of the *R* and *L* states, thus it has more energy compared to the case of initial condition (ii). As a result, the vibrational bath has a slighty higher effective temperature in this case, causing faster damping of the oscillatory population dynamics. The slower dynamics that arise with smaller J values are less susceptible to effects brought about by the initial distribution of the vibrational modes, as the bath equilibrates on a time scale faster than the electronic motion in this case.

The population curves in Fig. 4 do not have the familiar smooth curvature commonly seen in spin-boson dynamics with model spectral densities. (For example, the red data points in Fig. 4a have the appearance of a hand-drawn curve.) As evidenced by the small size of the error bars, these features are not a consequence of Monte Carlo noise, and they are not the result of numerical error. Rather, they are a manifestation of the richness of the true BChl normal mode spectral density, which is characterized by wildly varying Huang-Rhys factors. These characteristics cannot be captured by simple, analytic spectral density functions defined in terms of just two or three parameters, and thus they have not been observed in previous theoretical calculations. The complexity of time scales in the BChl dimer vibrational bath is more prominent in the early time dynamics, in particular in the case of initial condition (i) which corresponds to an initially unrelaxed (i.e. more energetic) bath. As time progresses, relaxation of the bath leads to smoother dynamics. The population curves obtained with smaller J values exhibit slower oscillations, and the early effects of the unrelaxed multimode bath are less noticeable.

Upon close examination, the envelop of the oscillations in $P(t)$ obtained with the higher J values is seen to follow an unusual nonexponential pattern, i.e. the population at the second recurrence is only slightly diminished compared to that at the first recurrence. Again, this trend is different from that

observed in typical spin-boson calculations with analytical spectral densities. The observed behavior is a consequence of the very long memory of the BChl vibrational bath. As the value of J is decreased, the normal mode frequency distribution is effectively higher, leading to less dramatic memory effects.

Next, we examine the effects of static disorder for the calculated electronic coupling value $J = 315\,\mathrm{cm}^{-1}$.[36] In Figure 5 we show the excited state population of pigment A for the asymmetric dimer Hamiltonian modeling static disorder. The energy splitting is now given by $2\sqrt{J^2+\varepsilon^2}$. As expected, strongly asymmetric configurations give rise to localized eigenstates of the singly excited Hamiltonian, which disrupt the tunneling dynamics, leading to only mildly oscillatory evolution.

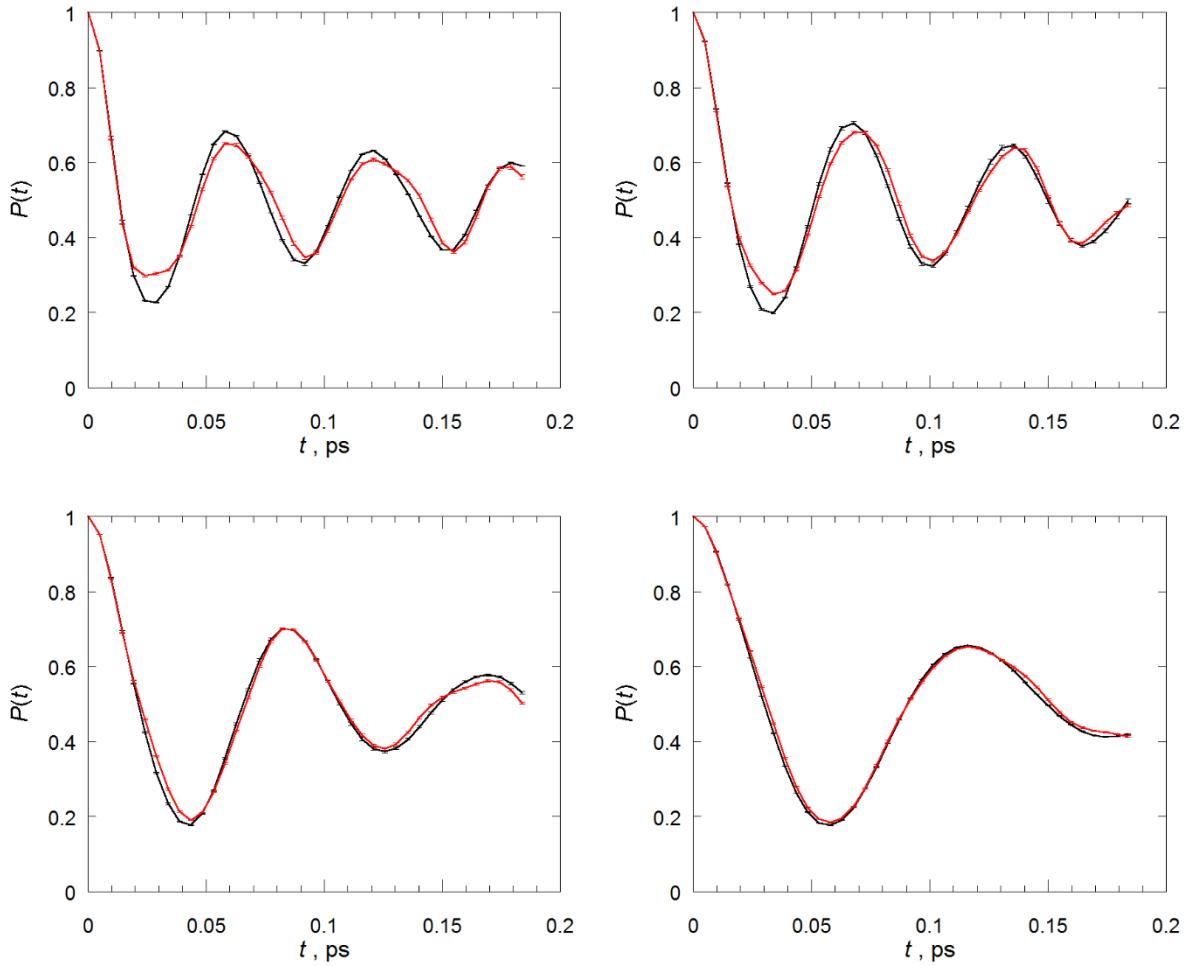

Fig. 4. Excited state population of pigment A in a symmetric dimer as a function of time at T = 300 K. Red and black correspond to vibrational initial conditions (i) and (ii), respectively. Top left: $J = 363\,\mathrm{cm}^{-1}$. Top right: $J = 315\,\mathrm{cm}^{-1}$. Bottom left: $J = 245\,\mathrm{cm}^{-1}$. Bottom right: $J = 181\,\mathrm{cm}^{-1}$. The Monte Carlo error bars indicate one standard deviation.

Figure 6 shows the averaged population with respect to the Gaussian distribution with mean asymmetry parameter $\bar{\varepsilon} = 0$, and compares to the population of the symmetric dimer. It is seen that static

disorder leads to a slight blue shift of the central frequency and considerable damping of the oscillation. Similar results are presented in Figure 7 for asymmetry distributions with mean $\bar{\varepsilon} = \pm 151.8\,\mathrm{cm}^{-1}$. In all cases, the effects of different bath initial conditions are still noticeable in the averaged population dynamics.

Our results show no evidence of EET enhancement by a vibrational mode resonant with the electronic transition energy.[23] Instead, the change in the population dynamics is the collective result of all coupled vibrational modes, and the main effect is damping of the oscillations.

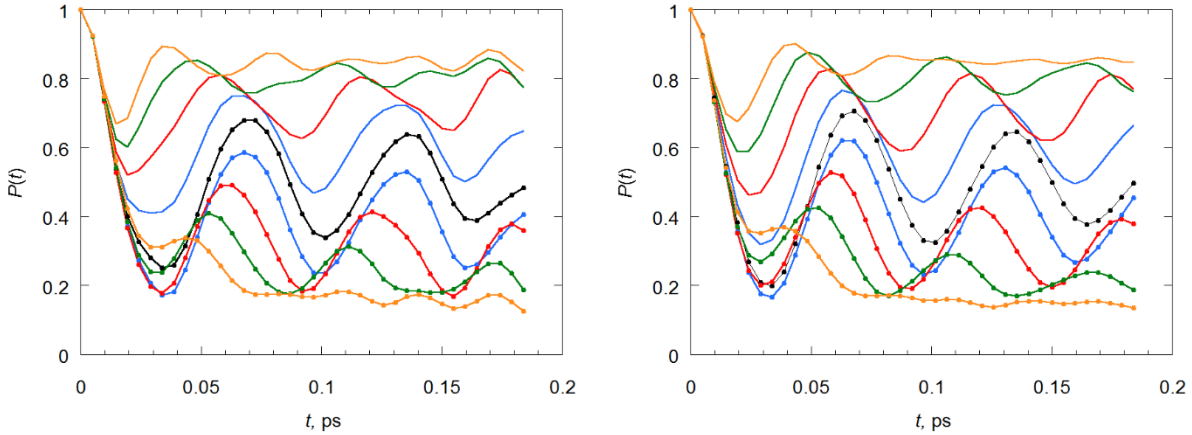

Fig. 5. Excited state population of pigment A as a function of time at T = 300 K for various value of the disorder parameter with $J = 315\,\mathrm{cm}^{-1}$. Black, $\varepsilon = 0$; blue, $\varepsilon = \pm 151.8\,\mathrm{cm}^{-1}$; red: $\varepsilon = \pm 303.7\,\mathrm{cm}^{-1}$; green: $\varepsilon = \pm 456.1\,\mathrm{cm}^{-1}$; orange: $\varepsilon = \pm 609.2\,\mathrm{cm}^{-1}$. Lines with dots correspond to positive values of ε. Left: initial condition (i). Right: initial condition (ii).

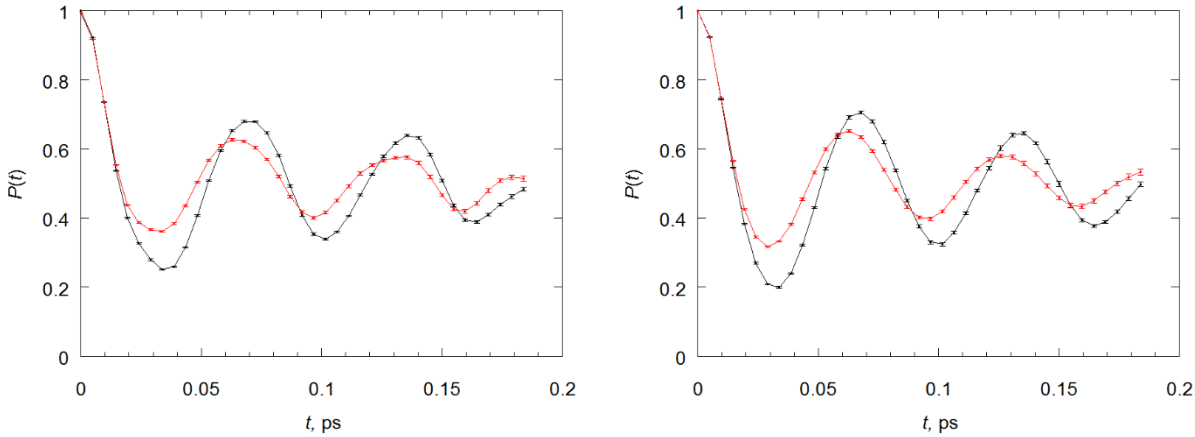

Fig. 6. Excited state population of pigment A with $J = 315\,\mathrm{cm}^{-1}$ at T = 300 K. Black: symmetric dimer, $\varepsilon = 0$. Red: population averaged with respect to the static disorder parameter with mean value $\bar{\varepsilon} = 0$. Left: initial condition (i). Right: initial condition (ii).

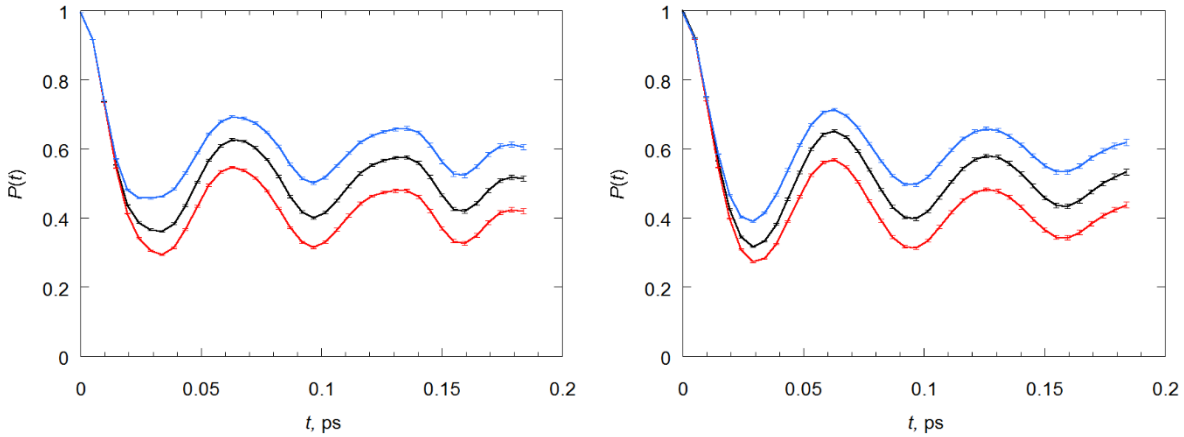

Fig. 7. Excited state population of pigment A, averaged with respect to the static disorder parameter, with $J = 315\,\mathrm{cm}^{-1}$ at $T = 300$ K. Black: mean of static disorder distribution at $\varepsilon = 0$. Blue: : mean of static disorder distribution at $\bar{\varepsilon} = -151.8\,\mathrm{cm}^{-1}$. Red: mean of static disorder distribution at $\bar{\varepsilon} = 151.8\,\mathrm{cm}^{-1}$. Left: initial condition (i). Right: initial condition (ii).

VII. Discussion and concluding remarks

In this paper we have presented numerically exact, fully quantum mechanical simulations of EET dynamics in BChl dimers, where all 50 coupled vibrational modes of each BChl accounted for with the precise parameters obtained from experimental Huang-Rhys factors. To our knowledge, the present study is the first to treat all BChl normal modes explicitly with spectroscopic accuracy. By avoiding the use of model spectral densities, which can alter significantly the characteristics of the vibrational modes, our results provide a quantitative picture of exciton-vibration dynamics in BChl dimers. The population curves exhibit characteristics that are not present in earlier calculations employing model spectral densities. These features stem from the complexity of the BChl vibrational bath.

The transformation presented in sections II and III shows that the Hamiltonian for the BChl dimer, where the electonic states are coupled by Frenkel exciton terms, and each electronic state includes the vibrational normal modes of each pigment, can be mapped exactly on the familiar spin-boson Hamiltonian where the two sites are coupled to a common bath of modes with rescaled parameters. Initial conditions reflecting a Franck-Condon excitation or a vibrational state pre-equilibrated with the excited BChl are mapped, respectively, to unshifted and shifted bath initial conditions.

The work presented here focuses on an isolated BChl dimer, for which the QCPI results presented in section VI show that the excitation energy oscillates persistently between the two pigments under physiological conditions. Static disorder arises from $\omega \to 0$ degrees of freedom of the environment, whose slow modulation compared to the TLS dynamics is equivalent to an ensemble of asymmetric TLS configurations. Asymmetry tends to cause a suppression of tunneling, leading to some damping of the oscillations. We emphasize that the static disorder treament of the medium is incapable of accounting for the dissipative role of phonon-like modes in the actual protein enviroment. Thus, if the dimer were to be embedded in its protein scaffold, the additional dynamic disorder from the dephasing effects of sluggish protein motion would lead to further suppression of the oscillatory features in the population dynamics.

Calculations investigating the effects of the protein enviroment found in light harvesting systems, monitoring the relaxation following excitation of an electronic eigenstate of the dimer, and also exploring the EET dynamics in longer BChl chains and rings, will be reported in future papers by our group.

Acknowledgment

This material is based upon work supported by the National Science Foundation under Award CHE-1665281.

References

1. Valkunas, L.; Amerongen, H. V.; Van Grondelle, R., *Photosynthetic excitons*. World Scientific: 2000.
2. Blankenship, R. E., *Molecular mechanisms of photosynthesis*. World Scientific: London, 2002.
3. Fenna, R. E.; Matthews, B. W., Chlorophyll arrangement in a bacteriochlorophyll protein from Chlorobium limicola. *Nature* **1975**, 258, 573-577.
4. Camara-Artigas, A.; Blankenship, R. E.; Allen, J. P., The structure of the FMO protein from Chlorobium tepidum at 2.2 Å resolution. *Photosynthesis Research* **2003**, 75, 49-55.
5. Goedheer, J. C., Temperature dependence of absorption and fluorescence spectra of bacteriochlorophylls in vivo and in vitro. *Biochim. Biophys. Acta* **1972**, 275, 169.
6. Evans, T. A.; Katz, J. J., Evidence for 5- and 6-coordinated magnesium in bacteriochlorophyll a from visible absorption spectroscopy. *Biochimica et Biophysica Acta* **1975**, 396, 414-426.
7. Avarmaa, R. A.; Rebane, K. K., High-resolution optical spectra of chlorophyll molecules. *Spectrochimica Acta A* **1985**, 41, 1365-1380.
8. van der Laan, H.; Smorenburg, H. E.; Schmidt, T.; Völker, S., Permanent hole burning with a diode laser: excited-state dynamics of bacteriochlorophyll in glasses and micelles. *J. Opt. Soc. Am. B* **1992**, 9, 931-940.
9. Cherepy, N. J.; Shreve, A. P.; Moore, L. J.; Boxer, S. G.; Mathies, R. A., Electronic and Nuclear Dynamics of the Accessory Bacteriochlorophylls in Bacterial Photosynthetic Reaction Centers from Resonance Raman Intensities. *The Journal of Physical Chemistry B* **1997**, 101, 3250-3260.
10. Wendling, M.; Pullerits, T.; Przyjalgowski, M. A.; Vulto, S. I. E.; Aartsma, T. J.; van Grondelle, R.; van Amerongen, H., Electron−Vibrational Coupling in the Fenna−Matthews−Olson Complex of Prosthecochloris aestuarii Determined by Temperature-Dependent Absorption and Fluorescence Line-Narrowing Measurements. *The Journal of Physical Chemistry B* **2000**, 104, 5825-5831.
11. Book, L. D.; Ostafin, A. E.; Ponomarenko, N.; Norris, J. R.; Scherer, N. F., Exciton Delocalization and Initial Dephasing Dynamics of Purple Bacterial LH2. *The Journal of Physical Chemistry B* **2000**, 104, 8295-8307.
12. Zazubovich, V.; Tibe, I.; Small, G. J., Bacteriochlorophyll a Franck−Condon Factors for the S0 → S1(Qy) Transition. *The Journal of Physical Chemistry B* **2001**, 105, 12410-12417.
13. Rätsep, M.; Cai, Z.-L.; Reimers, J. R.; Freiberg, A., Demonstration and interpretation of significant asymmetry in the low-resolution and high-resolution Qy fluorescence and absorption spectra of bacteriochlorophyll a. *J. Chem. Phys.* **2011**, 134, 024506.
14. Savikhin, S.; Buck, D. R.; Struve, W. S., Oscillating anisotropies in a bacteriochlorophyll protein: Evidence for quantum beating between exciton levels. *Chem. Phys.* **1997**, 223, 303-312.
15. Jonas, D. M., Two-dimensional femtosecond spectroscopy. *Annu. Rev. Phys. Chem.* **2003**, 54, 425-463.
16. Brixner, T.; T., M.; Stiopkin, I. V.; Fleming, G. R., Phase-stabilized two-dimensional electronic spectroscopy *J. Chem. Phys.* **2004**, 121, 4221.
17. Engel, G. S.; Calhoun, T. R.; Read, E. L.; Ahn, T.-K.; Mančal, T.; Cheng, Y.-C.; Blankenship, R. E.; Fleming, G. R., Evidence for wavelike energy transfer through quantum coherence in photosynthetic systems. *Nature* **2007**, 446, 782-786.
18. Calhoun, T. R.; Ginsberg, N. S.; Schlau-Cohen, G. S.; Cheng, Y.-C.; Ballottari, M.; Bassi, R.; Fleming, G. R., Quantum Coherence Enabled Determination of the Energy Landscape in Light-Harvesting Complex II. *The Journal of Physical Chemistry B* **2009**, 113, 16291-16295.
19. Ishizaki, A.; Fleming, G. R., Theoretical examination of quantum coherence in a photosynthetic system at physiological temperature. *Proceedings of the National Academy of Sciences* **2009**, 106, 17255-17260.
20. Strümpfer, J.; Schulten, K., Light harvesting complex II B850 excitation dynamics. *The Journal of Chemical Physics* **2009**, 131, 225101.

21. Collini, E.; Wong, C. Y.; Wilk, K. E.; Curmi, P. M. G.; Brumer, P.; Scholes, G. D., Coherently wired light-harvesting in photosyntheticmarine algae at ambient temperature. *Nature* **2010**, 463, 644.
22. Renger, T.; May, V.; Kuhn, O., Ultrafast excitation energy transfer dynamics in photosynthetic pigment–protein complexes. *Phys. Rep.* **2001**, 343, 137-254.
23. Tiwari, V.; Peters, W. K.; Jonas, D. M., Electronic resonance with anticorrelated pigment vibrations drives photosynthetic energy transfer outside the adiabatic framework. *Proc. Nat. Acad Sci. USA* **2013**, 110, 1203-1208.
24. Tiwari, V.; Peters, W. K.; Jonas, D. M., Electronic energy transfer through non-adiabatic vibrational-electronic resonance. I. Theory for a dimer. *J. Chem. Phys.* **2017**, 147, 154308.
25. Duan, H.-G.; Prokhorenko, V. I.; Cogdell, R. J.; Ashraf, K.; Stevens, A. L.; Thorwart, M.; Miller, R. J. D., Nature does not rely on long-lived electronic quantum coherence for photosynthetic energy transfer. *Proceedings of the National Academy of Sciences* **2017**, 201702261.
26. Worster, S. B.; Stross, C.; Vaughan, F. M. W. C.; Linden, N.; Manby, F. R., Structure and Efficiency in Bacterial Photosynthetic Light Harvesting. *The Journal of Physical Chemistry Letters* **2019**, 10, 7383-7390.
27. Arsenault, E. A.; Yusuke, Y.; Iwai, M.; Niyogi, K. K.; Fleming, G. R., Vibronic mixing enables ultrafast energy flow in light-harvesting complex II. *Nature Communications* **2020**, 11, 1460.
28. Kuhn, O.; Renger, T.; May, V.; Voigt, J.; Pullerits, T.; Sundstrom, V., Exciton-vibrational coupling in photosynthetic antenna complexes: theory meets experiment. *Trends in Photochemistry & Photobiology* **1997**, 4, 213-256.
29. Tretiak, S.; Middleton, C.; Chernyak, V.; Mukamel, S., Exciton Hamiltonian for the bacteriochlorophyll system in the LH2 antenna complex of purple bacteria. *J. Phys. Chem. B* **2000**, 104, 4519-4528.
30. Tretiak, S.; Middleton, C.; Chernyak, V.; Mukamel, S., Bacteriochlorophyll and carotenoid excitonic couplings in the LH2 system of purple bacteria. *J. Phys. Chem. B* **2000**, 104, 9540-9553.
31. Adolphs, J.; Renger, T., How proteins trigger excitation energy transfer in the FMO complex of green sulfur bacteria. *Biophys J.* **2006**, 91, 2778–2797.
32. Ishizaki, A.; Fleming, G. R., Unified treatment of quantum coherent and incoherent hopping dynamics in electronic energy transfer: Reduced hierarchy equation approach. *The Journal of Chemical Physics* **2009**, 130, 234111.
33. Abramavicius, D.; Mukamel, S., Quantum oscillatory exciton migration in photosynthetic reaction centers. *J. Chem. Phys.* **2010**, 133, 064510.
34. Tao, G.; Miller, W. H., Semiclassical description of electronic excitation population transfer in a model photosynthetic system. *J. Phys. Chem. Lett.* **2010**, 1, 891-894.
35. Huo, P.; Coker, D. F., Iterative linearized density matrix propagation for modeling coherent excitation energy transfer in photosynthetic light harvesting. *J. Chem. Phys.* **2010**, 133, 184108.
36. Strümpfer, J.; Schulten, K., The effect of correlated bath fluctuations on exciton transfer. *The Journal of Chemical Physics* **2011**, 134, 095102.
37. Nalbach, P.; Ishizaki, A.; Fleming, G. R.; Thorwart, M., Iterative path-integral algorithm versus cumulant time-nonlocal master equation approach for dissipative biomolecular exciton transport. *New Journal of Physics* **2011**, 13, 063040.
38. Nalbach, P.; Braun, D.; Thorwart, M., Exciton transfer dynamics and quantumness of energy transfer in the Fenna-Matthews-Olson complex. *Phys. Rev. E* **2011**, 84, 041926.
39. Liang, X.-T., Simulating signatures of two-dimensional electronic spectra of the Fenna-Matthews-Olson complex: By using a numerical path integral. *The Journal of Chemical Physics* **2014**, 141, 044116.
40. Yeh, S.-H.; Hoehn, R. D.; Allodi, M. A.; Engel, G. S.; Kais, S., Elucidation of near-resonance vibronic coherence lifetimes by nonadiabatic electronic-vibrational state character mixing. *Proceedings of the National Academy of Sciences* **2019**, 116, 18263-18268.

41. Bhattacharyya, P.; Fleming, G. R., Two-Dimensional Electronic–Vibrational Spectroscopy of Coupled Molecular Complexes: A Near-Analytical Approach. *The Journal of Physical Chemistry Letters* **2019**, 10, 2081-2089.
42. Mukamel, S., *Principles of nonlinear optical spectroscopy*. Oxford University Press: New York, 1995.
43. Redfield, A. G., On the theory of relaxation processes. *IBM Journal of Research and Development* **1957**, 1, 19-31.
44. Pollard, W. T.; Felts, A. K.; Friesner, R. A. The Redfield Equation in Condensed-Phase Quantum Dynamics. In *Advances in Chemical Physics*; 1996; Vol. 93, pp 77-134.
45. Meyer, H.-D.; Miller, W. H., A classical analog for electronic degrees of freedom in nonadiabatic collision processes. *J. Chem. Phys.* **1979**, 70, 3214-3223.
46. Stock, G.; Thoss, M., Semiclassical description of nonadiabatic quantum dynamics. *Phys. Rev. Lett.* **1997**, 78, 578-581.
47. Wang, H.; Sun, X.; Miller, W. H., Semiclassical approximations for the calculation of thermal rate constants for chemical reactions in complex molecular systems. *J. Chem. Phys.* **1998**, 108, 9726-9736.
48. Ishizaki, A.; Tanimura, Y., Quantum Dynamics of System Strongly Coupled to Low-Temperature Colored Noise Bath: Reduced Hierarchy Equations Approach. *Journal of the Physics Society Japan* **2005**, 74, 3131-3134.
49. Feynman, R. P., Space-time approach to non-relativistic quantum mechanics. *Rev. Mod. Phys.* **1948**, 20, 367-387.
50. Feynman, R. P.; Hibbs, A. R., *Quantum Mechanics and Path Integrals*. McGraw-Hill: New York, 1965.
51. Vega, I. D.; Alonso, D., Dynamics of non-Markovian open quantum systems. *Rev. Mod. Phys.* **2017**, 89, 015001.
52. Feynman, R. P.; F. L. Vernon, J., The theory of a general quantum system interacting with a linear dissipative system. *Ann. Phys.* **1963**, 24, 118-173.
53. Makri, N., Improved Feynman propagators on a grid and non-adiabatic corrections within the path integral framework. *Chem. Phys. Lett.* **1992**, 193, 435-444.
54. Makri, N.; Makarov, D. E., Tensor multiplication for iterative quantum time evolution of reduced density matrices. I. Theory. *J. Chem. Phys.* **1995**, 102, 4600-4610.
55. Makri, N.; Makarov, D. E., Tensor multiplication for iterative quantum time evolution of reduced density matrices. II. Numerical methodology. *J. Chem. Phys.* **1995**, 102, 4611-4618.
56. Sim, E.; Makri, N., Filtered propagator functional for iterative dynamics of quantum dissipative systems. *Comp. Phys. Commun.* **1997**, 99, 335-354.
57. Sim, E., Quantum dynamics for a system coupled to slow baths: on-the-fly filtered propagator method. *J. Chem. Phys.* **2001**, 115, 4450-4456.
58. Lambert, R.; Makri, N., Memory path propagator matrix for long-time dissipative charge transport dynamics. *Mol. Phys.* **2012**, 110, 1967-1975.
59. Makri, N., Path integral renormalization for quantum dissipative dynamics with multiple timescales. *Mol. Phys.* **2012**, 110, 1001-1007.
60. Richter, M.; Fingerhut, B. P., Coarse-grained representation of the quasiadiabatic propagator path integral for the treatment of non-Markovian long-time bath memory. *J. Chem. Phys.* **2017**, 146, 214101.
61. Strathearn, A.; Kirton, P.; Kilda, D.; Keeling, J.; Lovett, B. W., Efficient non-Markovian quantum dynamics using time-evolving matrix product operators. *Nature Communications* **2018**, 9, 3322.
62. Makri, N., Blip decomposition of the path integral: Exponential acceleration of real-time calculations for quantum dissipative systems. *J. Chem. Phys.* **2014**, 141, 134117.
63. Makri, N., Iterative blip-summed path integral for quantum dynamics in strongly dissipative environments. *J. Chem. Phys.* **2017**, 146, 134101.
64. Makri, N., Small matrix disentanglement of the path integral: overcoming the exponential tensor scaling with memory length. *J. Chem. Phys.* **2020**, 152, 041104.

65. Donoso, A.; Martens, C. C., Simulation of coherent nonadiabatic dynamics using classical trajectories. *J. Phys. Chem. A* **1998**, 102, 4291.
66. Kapral, R.; Ciccotti, G., Mixed quantum-classical dynamics. *J. Chem. Phys.* **1999**, 110, 8919-8929.
67. Mac Kernan, D.; Ciccotti, G.; Kapral, R., Sequential short-time propagation of quantum-classical dynamics. *J. Phys. Cond. Matt.* **2002**, 14, 9069-9076.
68. Mac Kernan, D.; Ciccotti, G.; Kapral, R., Trotter based simulation of quantum-classical dynamics. *j . Phys. Chem. B* **2008**, 114.
69. Ehrenfest, P., Bemerkung über die angenäherte Gültigkeit der klassischen Mechanik innerhalb der Quantenmechanik. *Z. Phys.* **1927**, 45, 455-457.
70. Lambert, R.; Makri, N., Quantum-classical path integral: Classical memory and weak quantum nonlocality. *J. Chem. Phys.* **2012**, 137, 22A552.
71. Lambert, R.; Makri, N., Quantum-classical path integral: Numerical formulation. *J. Chem. Phys.* **2012**, 137, 22A553.
72. Makri, N., Quantum-classical path integral: A rigorous approach to condensed phase dynamics. *International Journal of Quantum Chemistry* **2015**, 115, 1209-1214.
73. Walters, P. L.; Makri, N., Quantum-classical path integral simulation of the ferrocene-ferrocenium charge transfer in liquid hexane. *J. Phys. Chem. Lett.* **2015**, 6, 4959-4965.
74. Makri, N., Modular path integral methodology for real-time quantum dynamics. *J. Chem. Phys.* **2018**, 149, 214108.
75. Makri, N., Modular path integral: Quantum dynamics via sequential necklace linking. *J. Chem. Phys.* **2018**, 148, 101101.
76. Makri, N., Exploiting classical decoherence in dissipative quantum dynamics: Memory, phonon emission, and the blip sum. *Chem. Phys. Lett.* **2014**, 593, 93-103.
77. May, V.; Kühn, O., *Charge and energy transfer dynamics in molecular systems*. 3rd ed.; Wiley: 2011.
78. Frenkel, J., On the transfomation of light into heat in solids. *Phys. Rev.* **1931**, 37, 17.
79. Feynman, R. P., *Statistical Mechanics*. Addison-Wesley: Redwood City, 1972.
80. Freiberg, A.; Rätsep, M.; Timpmann, K.; Trinkunas, G., Excitonic polarons in quasi-one-dimensional LH1 and LH2 bacteriochlorophyll *a* antenna aggregates from photosynthetic bacteria: A wavelength-dependent selective spectroscopy study. *Chem. Phys.* **2009**, 357, 102-112.
81. Banerjee, T.; Makri, N., Quantum-classical path integral with self-consistent solvent-driven propagators. *J. Phys. Chem.* **2013**, 117, 13357-13366.
82. Walters, P. L.; Makri, N., Iterative quantum-classical path integral with dynamically consistent state hopping. *J. Chem. Phys.* **2016**, 144, 044108.
83. Metropolis, N.; Rosenbluth, A. W.; Rosenbluth, M. N.; Teller, H.; Teller, E., Equation of state calculations by fast computing machines. *J. Chem. Phys.* **1953**, 21, 1087-1092.
84. Makri, N., Blip-summed quantum-classical path integral with cumulative quantum memory. *Faraday Discuss.* **2016**, 195, 81-92.
85. Wang, F.; Makri, N., Quantum-classical path integral with a harmonic treatment of the back-reaction. *J. Chem. Phys.* **2019**, 150, 184102.